Wind wave source functions in opposing seas

Article *in* Journal of Geophysical Research: Oceans · August 2015

DOI: 10.1002/2015JC010816

Sabique Langodan
King Abdullah University of Science and Tech…

Yesubabu V
National Atmospheric Research Laboratory

AGU PUBLICATIONS

JGR

Journal of Geophysical Research: Oceans

RESEARCH ARTICLE

10.1002/2015JC010816

Key Points:

- Evolution and propagation of opposing wind waves with similar characteristics
- Available wave model source functions may not properly model this situation
- Proposed and tested a solution to improve wave simulation under opposing seas

Correspondence to:
I. Hoteit,
ibrahim.hoteit@kaust.edu

Citation:
Langodan, S., L. Cavaleri, Y. Viswanadhapalli, and I. Hoteit (2015), Wind-wave source functions in opposing seas, *J. Geophys. Res. Oceans*, *120*, doi:10.1002/2015JC010816.

Received 9 MAR 2015
Accepted 24 AUG 2015
Accepted article online 26 AUG 2015

Wind-wave source functions in opposing seas

Sabique Langodan[1], Luigi Cavaleri[2], Yesubabu Viswanadhapalli[1,3], and Ibrahim Hoteit[1]

[1]Physical Science and Engineering Division, King Abdullah University of Science and Technology, Thuwal 23955-6900, Saudi Arabia, [2]Institute of Marine Sciences, Venice, Italy, [3]National Atmospheric Research Laboratory (NARL), Department of Space (DoS), Govt. of India, Gadanki - 517 112, Chittoor District, Andhra Pradesh

Abstract The Red Sea is a challenge for wave modeling because of its unique two opposed wave systems, forced by opposite winds and converging at its center. We investigate the different physical aspects of wave evolution and propagation in the convergence zone. The two opposing wave systems have similar amplitude and frequency, each driven by the action of its own wind. Wave patterns at the center of the Red Sea, as derived from extensive tests and intercomparison between model and measured data, suggest that the currently available wave model source functions may not properly represent the evolution of the local fields that appear to be characterized by a less effective wind input and an enhanced white-capping. We propose and test a possible simple solution to improve the wave-model simulation under opposing winds and waves condition.

1. The Problem to be Discussed

The remarkable progress of wind-wave modeling in the last few decades is mainly due to two reasons: (a) substantial improvements to the quality and resolution of meteorological modeling and (b) a keen definition of the source functions in the wave models. *The WISE Group* [2007] has made a comprehensive panorama of the situation and documented the state-of-the-art approaches. More recent developments are presented in *Ardhuin et al*. [2010].

While we have reasons to be pleased with the successes in the field (see e.g., *Janssen* [2008] and the statistics of the European Centre for Medium-Range Weather Forecasts, henceforth ECMWF, at www.ecmwf.int), it is important to remember how we arrived at the presently working theory of the single processes of wave modeling, in particular the generation by wind and white-capping. The basic idea of wind-wave evolution theories, see *Miles* [1957] and *Janssen* [1991] for the former or *Hasselmann* [1974] and *Komen et al*. [1984] for the latter, is that of a wind sea (typically a JONSWAP spectrum [*Hasselmann et al*., 1973]) eventually reaching a well-developed stage. As one may expect, application to a real ocean with different wave systems (for energy, period, and direction) acting simultaneously, forced some revisits of the mechanisms as, among others, those by *Bidlot et al*. [2007], *Ardhuin et al*. [2010], and *Babanin* [2011]. However, subsequent modulations serve more as updates than a reform of the basis of the original idea. This is particularly true for white-capping, which remains the least understood part of wind-wave dynamics, and as such is used in practice as the tuning knob of the system. Conflicting results reflect our insufficient knowledge of the involved physical mechanisms.

In this study, we investigate whether the two generally accepted source functions that contribute, with their positive and negative terms, to the overall energy budget of the system remain valid in conditions very different from the ones typically found in the oceans. We begin by considering an unusual meteorological, hence wave, situation, which will be described later and that occurs in the Red Sea, where we are focusing our attention. An extensive application of an advanced third-generation wave model and analysis of available data in the region will provide information for a useful discussion. The study is organized as follows: section 2 describes the study area, the Red Sea; section 3 describes the focus of the work and details relevant to our tests; section 4 briefly outlines the modeling approach and the available data; section 5 compares model outputs with measured data; section 6 discusses the results, outlining the limits of the present formulations; and section 7 concludes our investigation and tentatively proposes an initial approach to a solution.

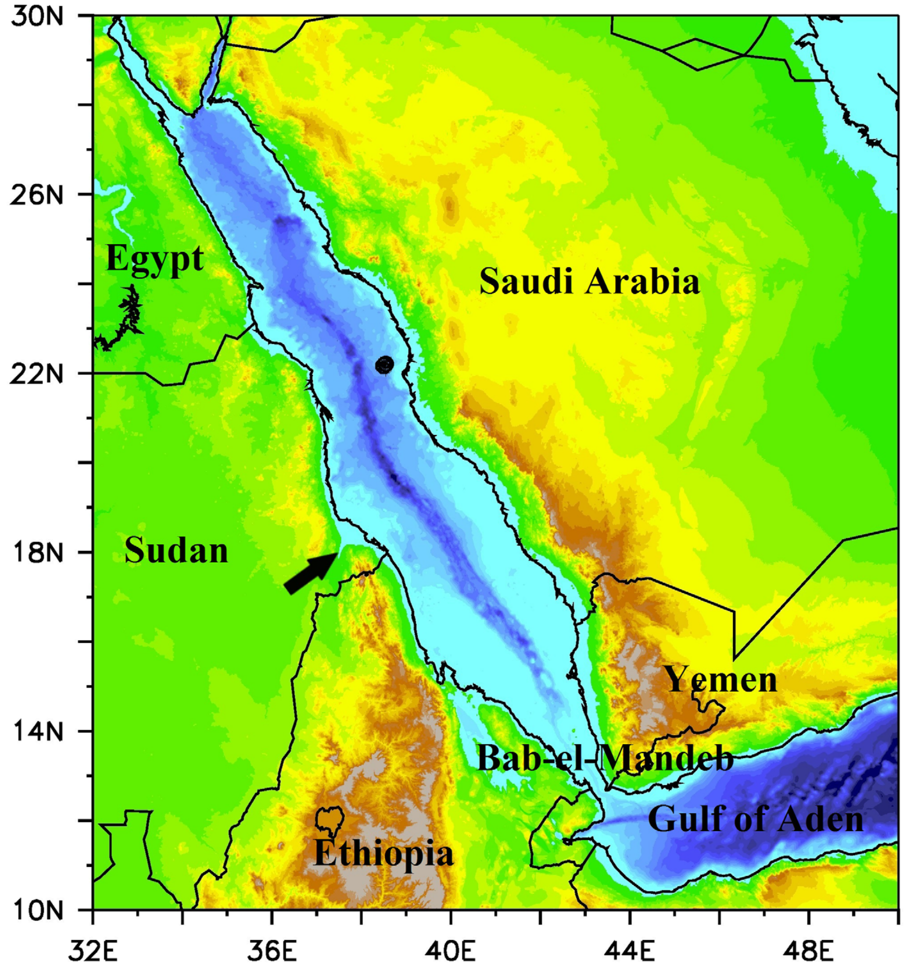

Figure 1. Orography and bathymetry of the Red Sea basin. The black dot indicates the position of the buoy used in this study. The arrow indicates the location of the Tokar Gap.

2. Characterization of the Area

2.1. Geography

The Red Sea is a narrow elongated basin (roughly 2000 $\times$ 200 km^2) distributed in the NNW-SSE direction (see Figure 1) between 10°N and 30°N latitude and 32°E and 44°E longitude. Closed at its northern end, it is connected at its southern end to the Gulf of Aden and the Arabian Sea via the narrow Bab el Mandeb strait. The average depth is 490 m, with peak values at more than 2000 m [*Morcos*, 1970].

The geological origin (being close to the East African rift) gives rise to two continuous ranges of high mountains on both sides of the sea. Both ranges reach their maximum altitude in the southern part of the basin, with more than 2000 m altitude in the Arabian Peninsula to the East and above 4000 m on the African side. Some valleys, especially on the eastern side, cut through the range. On the African side, a remarkable feature (see the arrow in Figure 1) is the 110 km wide Tokar Gap, connecting the sea with Sudan's Boma Plateau [*Jiang et al*., 2009].

2.2. Winds

Langodan et al. [2014] provide a detailed description of the various meteorological situations. The described orography transforms the Red Sea into a virtual wind channel, where the along-axis winds are the dominant feature. In summer, this is given by the SSE-directed wind that covers the entire basin. To provide a more direct dynamic insight, we will refer to flow direction for both wind and waves; we will also refer to the two along-axis possible directions as NW and SE. A combination of night cooling on Sudan's Boma Plateau and katabatic effects lead to the so-called Tokar Gap wind, which blows toward the eastern side

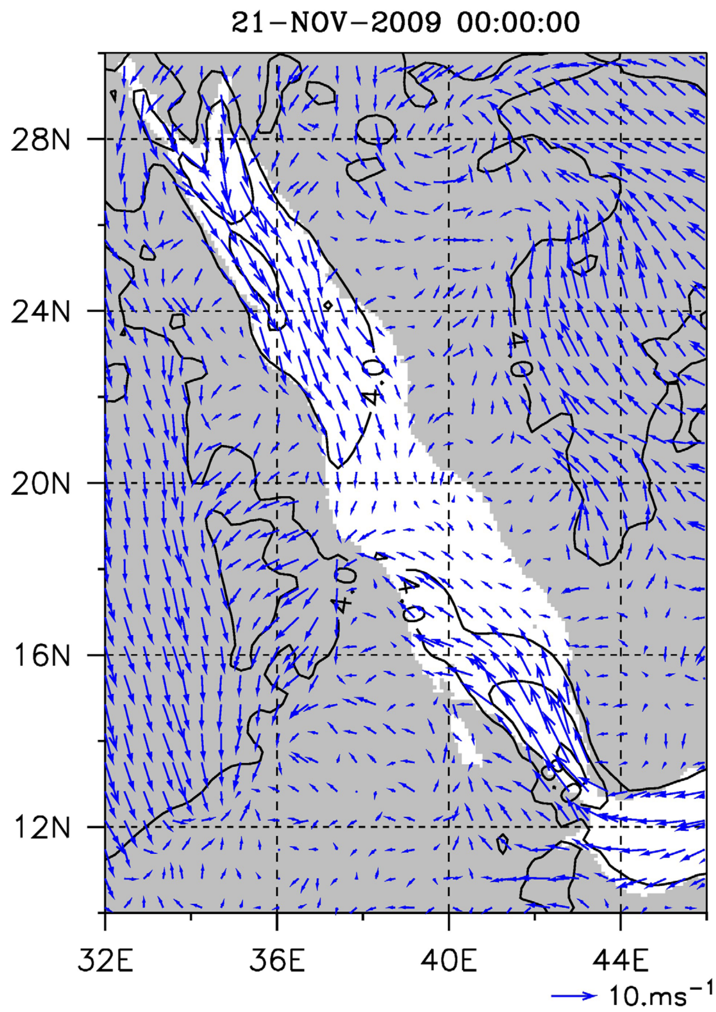

Figure 2. Convergence of SE-flowing and NW-flowing winds at the center of the Red Sea at 00 UTC 21 November 2009.

[*Jiang et al*., 2009]. Strong jets in the opposite direction erupt in some cases from the transversal valleys on the Arabian side of the sea.

The most uncommon set of conditions occurs in winter, typically between October and April, where both NW and SE winds are present. The NW wind arises from the WSW-blowing monsoon in the Gulf of Aden. Orographically forced through the Bab el Mandeb strait (see Figure 1), the wind is then channeled along the axis of the Red Sea. The SE winds typically originate from synoptic pulses of cold air from the Mediterranean Sea, just above the upper border in Figure 1. The simultaneous appearance of the NW and SE systems occurs in two slightly, but considerably different ways. The most common scenario is shown in Figure 2. Each of the two systems occupies a part of the surface of the Red Sea, with an intermediate zone of calm or weak winds. Figure 3 provides a vertical view of the situation; the warm NW flow slides on top of the cold northerly air flowing to the SE. Trapped in the Red Sea channel, the latter is forced to reverse, flowing back at higher altitude. Within the Red Sea convergence zone (CZ), the two airflows, both saturated with humidity, move to a higher altitude and cause an unusually cloudy zone with frequent drizzling in an otherwise ubiquitously sun dominated area. *Pedgley* [1996a,1996b] gives a full description of the region. The slight, but considerable difference occurs when the two systems come in contact without an intermediate calm zone. An example is shown in Figure 4, focused on the Tokar Gap area (see Figure 1 for its location). This typically happens when a previously dominating NW flow is vigorously pushed back by a sudden inflow of northerly air (moving SE). In this case, the separation line between the two systems acts as a cold front so that different winds are present at the surface on the two sides of the "front." The rapid advance of the cold front typically slows down at the latitude of the Tokar Gap, when the advancing cold air can escape to the west through the Gap (see Figure 4). It is these opposing winds that motivated this investigation.

2.3. Waves

Langodan et al. [2014] provide a full description of the wind-wave patterns in the Red Sea. Briefly, the NW and SE winds give rise to long fetch (up to 2000 km) fields that are not strong but are generally well developed. The narrow jets from the east coast lead to locally energetic young waves that have a strong transversal gradient. The katabatic Tokar Gap winds produce transversal flows that often interact with the summer dominant SE waves. The two opposed (NW and SE) coexisting winds produce two opposed wave systems with similar general characteristics. Here we focus on this unique situation and provides a more detailed description in the following section.

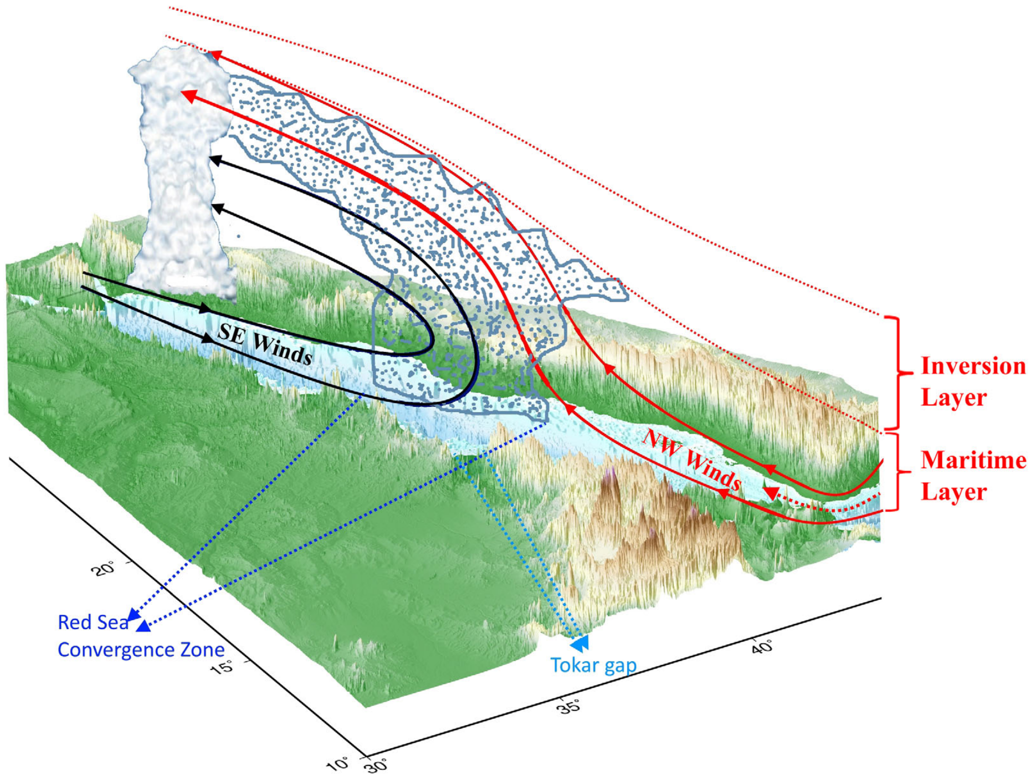

Figure 3. Vertical structure of the convergence zone shown in Figure 2. Wind flow directions are indicated.

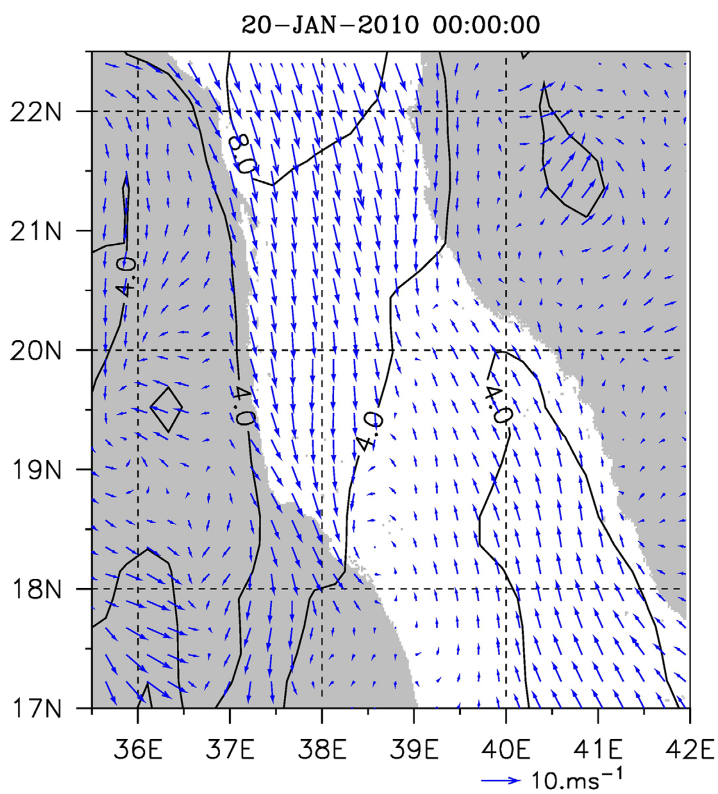

Figure 4. Convergence of two opposing wind systems at 00 UTC 20 January 2010. The south-flowing cold air funnels through the Tokar Gap (see Figure 1 for its position).

3. The Focus of the Work

We aim to illustrate, with data wherever possible, that some of the present assumptions for source functions in wave modeling require some modification to be applicable to less common oceanic conditions, particularly for the area and the wind systems studied here. Interestingly, although *Pedgley* [1996a,1996b] is an excellent source for referencing the wind patterns in the area, he was in fact investigating the migration of desert locusts. In 1966, wave modeling was still an art in its early stages, and unfortunately detailed local data are scarce. Nevertheless, we have an adequate amount of data to begin making a case for our point of view. Specifically, we focus on the source functions acting on the waves when considering two opposite similar active wave systems. We will begin by describing our modeling approach and the available data, and then we will discuss our results and suggest a possible suitable modification to the present-day model.

4. Model and Available Data

We refer to *Langodan et al*. [2014] for a full description of wind and wave modeling in the Red Sea. Here we report only the essential details relevant for the present discussion.

4.1. Wind Data

After testing several approaches, *Langodan et al*. [2014] showed that, based on the available information and on average, the best wind and wave results were obtained with a slightly enhanced ECMWF analysis wind fields. While highly precise in open oceans (see the cited ECMWF statistics), these surface fields tend to underestimate wind speed in enclosed seas, a typical feature of meteorological models [*Cavaleri and Bertotti*, 1997, 2004]. A careful guess and a few trial-and-error experiments suggested that a good solution would be to increase (in the Red Sea) the surface wind speed by 7%. Figure 5 shows four comparisons between enhanced wind speeds (indicated as ECMWF+) and derived wave heights versus the ASCAT scatterometer, altimeter (Jason-1, Jason-2, ENVISAT), and buoy data. The solution is clearly satisfactory, where the average difference from the ideal 45° best fit lines versus measured data is in the order of 1%. Note that for the comparison, the buoy wind data were considered at a 10 m height, assuming neutral conditions.

For our modeling purposes, we use the ECMWF analysis winds at 0.25° resolution, available at 6 h intervals (00, 06, 12, 18 UTC). Such a relatively large interval may mask, for example, accurate onsets of the katabatic Tokar Gap wind (see section 2), but it is sufficient for the northerly and southerly winds conditions we consider in this paper. Due to the strong insolation of the coasts, sea breezes can occasionally be intense, extending up to 100 km from the coast at their peak. Although sea breezes do not alter large-scale circulation, they do superimpose on the general flow.

4.2. Wave Model Outputs

We used the WAVEWATCH III model [*Tolman*, 2008, henceforth referred to as WW3] with both the BAJ formulation [*Bidlot et al*., 2007] and a more recent approach by *Ardhuin et al*. [2010], henceforth referred to as ARD. (This formulation is known as TEST451 parameterization or ST4 parameterization in latest version (v4.18) of the WAVEWATCH III model.) The model was configured on a 5 km resolution regular grid, lat-lon oriented, with 33 frequencies ($f_1 = 0.05$ Hz, $f_{n+1} = 1.1 \times f_n$) and 36 directions. The Discrete Interaction Approximation (DIA [*Hasselmann et al*., 1985], for the evaluation of the nonlinear wave-wave interaction term) was originally tuned to a 1.1 geometric progression of frequencies in 24 directions; any other approach would have required a different DIA calibration. In our case, there was no appreciable change in the nonlinear wave-wave interaction with an increased number of directions. Since BAJ and ARD approaches showed no noticeable change in the model simulation, we make no distinction in this respect. For the final data, both the two-dimensional spectra and the single-source functions were saved at hourly intervals for later analysis.

4.3. Available Observations

A meteo-oceanographic buoy located at 22°10′N, 38°30′E was operated from October 2008 until May 2010 at a local depth of 693 m. We used the Wave and Marine Data acquisition System (WAMDAS) developed by NOAA's National Data Buoy Center (NDBC) to obtain the meteo-oceanographic measurements. The details of the buoy can be found in *Teng et al*. [2005]. Its position (small black dot in Figure 1) was not ideal, being somehow shielded by the protruding coast with respect to waves coming from the southern part of the Red Sea. Data (wind speed and direction, two-dimensional spectra plus all the derived integrated quantities) are available at hourly intervals.

The Jason-1 altimeter passes over the Red Sea once every 10 days with a convenient ground track along the axis of the basin. The slightly shifted pass of Jason-2 is hardly usable, while the more inclined pass of ENVISAT also provided useful data, but over a shorter track. We used the quality-controlled and calibrated altimeter-derived values from the GlobWave database (http://www.globwave.org), and cross-checked them with the corresponding ones from RADS (http://rads.tudelft.nl/rads/rads.shtml). We used ASCAT

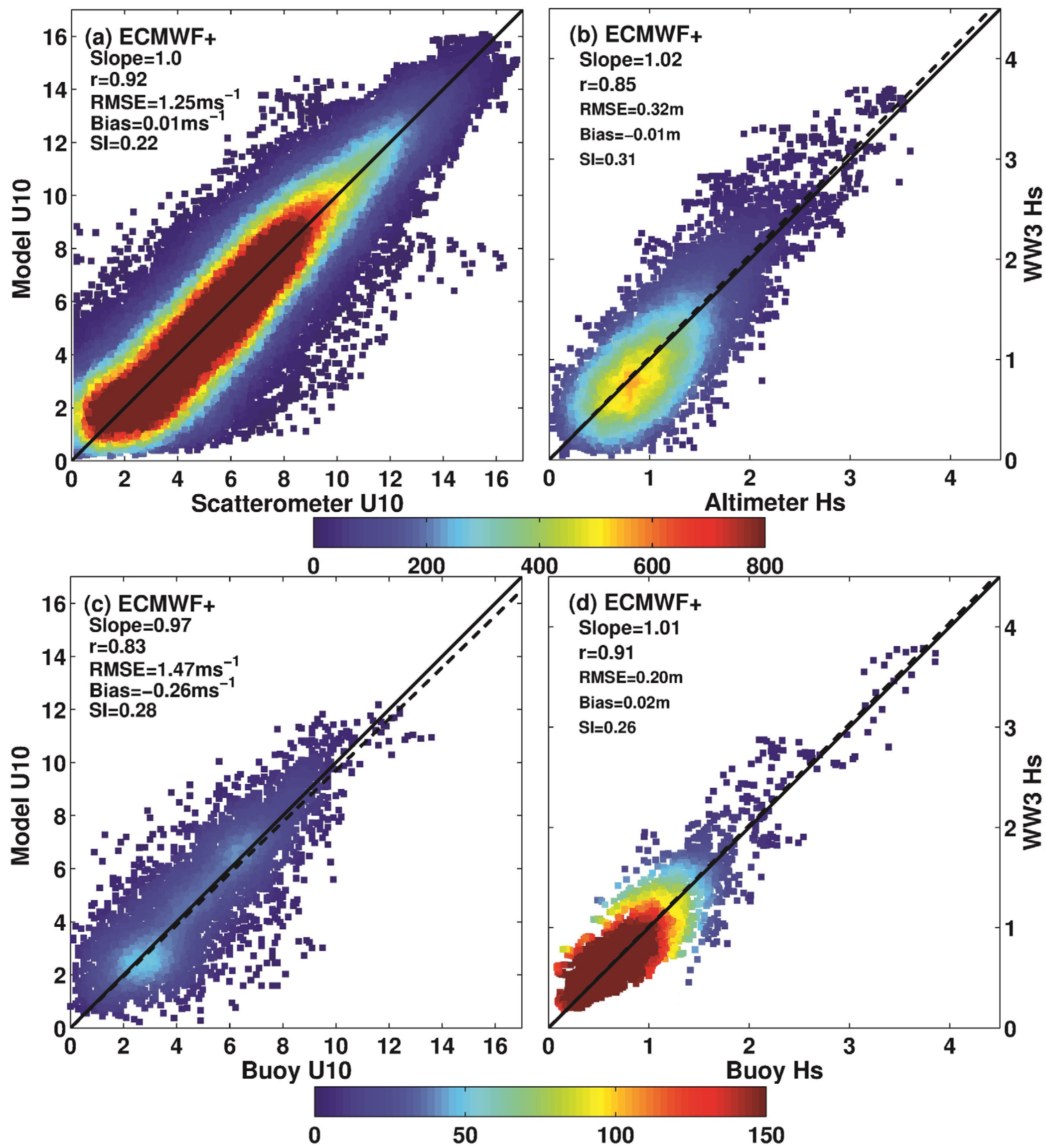

Figure 5. Best fits of enhanced (+7%) ECMWF wind speeds (+) and derived wave heights versus (top) scatterometer and altimeter and (bottom) buoy observed wind speed and wave height. Data collected between October 2009 and March 2010. The colors indicate the number of cases in each pixel.

scatterometer data extensively with two useful passes around 06 and 18 UTC over the upper and lower half of the basin, respectively.

We focused our study of the opposing wave conditions on the 2009–2010 winter season during a five month period (November–March).

5. Results of the Model and Their Comparison With Data

Figure 5 illustrates the overall performance of the meteorological and wave models. We focused on the CZ by visually inspecting the six hourly surface ECMWF wind maps (an example is in Figure 2) during the 5 month study time. We identified a well-defined CZ in 19 cases of convergence events. Our aim is to evaluate the wave-model performance during each of these cases with respect to the model overall performance over the whole domain. In particular, we explored the evolution of the two different wave systems (NW and

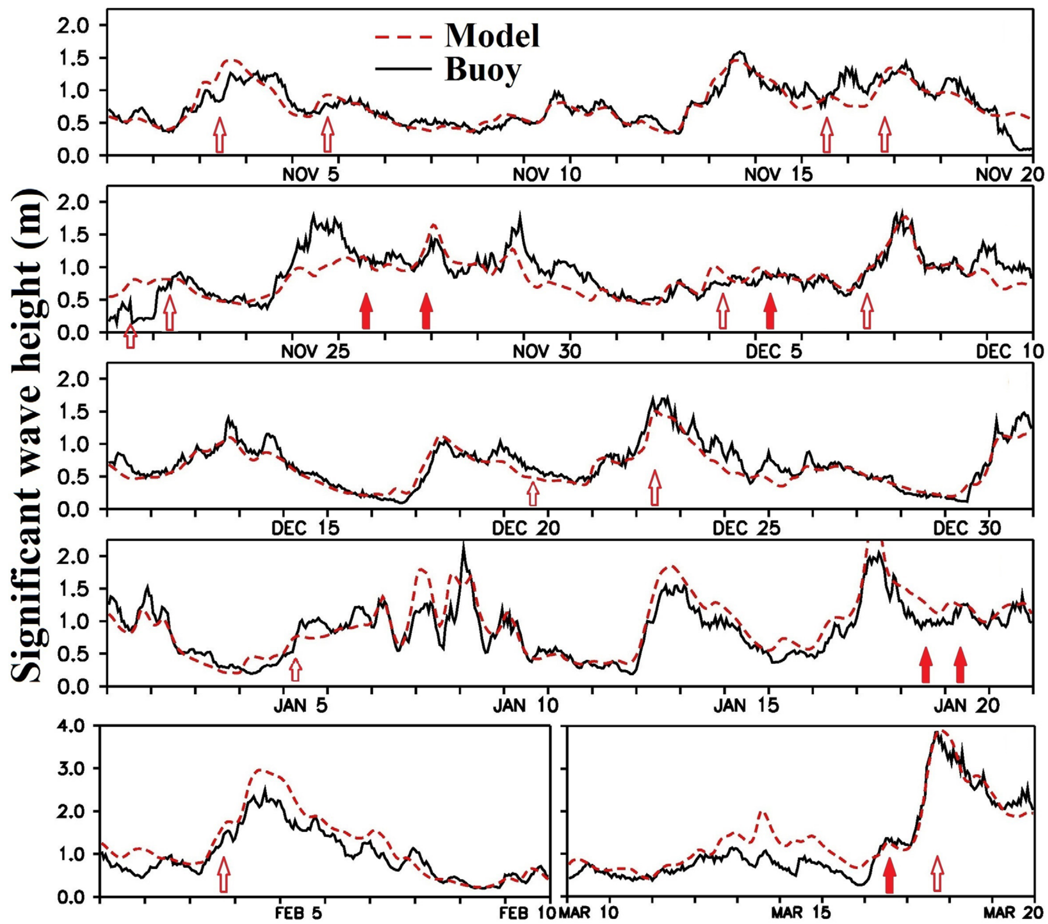

Figure 6. Time series plot of buoy and model simulated H_s from early November 2009 until late January 2010 and two cases in February and March, respectively. The arrows indicate the 19 cases analyzed in this study. The color-filled arrows indicate the six cases suitable for analysis.

SE). Inevitably, we focus on the buoy, the only location where all necessary information is available. The limited wavelengths in the Red Sea restricted us from looking for synthetic aperture radar spectra.

Figure 6 plots the time series of the measured and modeled significant wave height at the buoy location for 3 months (November–January) and for two short periods in February and March; the vertical arrows point to the CZ cases. Table 1 lists each CZ case, reports on model accuracy, and describes wind and wave behavior relative to the model and observations wherever available.

As it will be explained in the next section, we discuss the significant wave height, H_s, of the model to be too high when a CZ is present. A meaningful evaluation of model performance requires a considerable amount of quality wind field data; therefore, only cases with ample scatterometer data were considered. Furthermore, the bias of the modeled wind speeds and wave heights should not be macroscopically in the same direction (positive or negative). These conditions were necessary to draw conclusions. After considering these limitations, we focused on the only six cases where the conditions were satisfied. These are indicated by the color-filled arrows in Figure 6. Figure 7 provides zoomed-in view of three cases representative of possible situations. The second plot in Figure 7, representing 21 November, corresponds to the CZ shown in Figure 2.

To quantify the model errors with respect to errors in the wind speed, we have related the bias in the model H_s to the corresponding model surface wind. Using adimensional quantities, the former was evaluated as the average bias in the considered period (of a specific event), typically between 12 and 36 h, divided by the average buoy H_s over the same period. For the wind, the considered period was selected according to the meteorological conditions and the available scatterometer data. Figure 8 shows a scatterplot of the

Table 1. A List of the Strong Convergence Events Between October 2009 and March 2010, Their Characteristics, and a Compact Description of the Wind and Wave Models Performance

		Available Information	
Date	RSCZ Characteristics	Waves	Wind
3 Nov 2009	Large CZ in the south	Model overestimated	SE winds are dominant; model winds are underestimated
5 Nov 2009	Large CZ in the center	Model overestimated	Both winds are equal; model winds are very high in the south
16 Nov 2009	Large CZ at Tokar Gap (TG)	Model predicted well	No information about winds
17 Nov 2009	Large CZ at TG	Model underestimated	Model wind is too low, not usable
21 Nov 2009	Narrow CZ at TG	Model overestimated	Wind very weak in the south; model wind underestimated in the north
22–23 Nov 2009	Large CZ at TG	Model overestimated	SE winds are low; NW winds are low in the south
26 Nov 2009	Narrow CZ at TG	Model predicted well	Limited information about wind
27 Nov 2009	Narrow CZ at TG	Model overestimated	NW is dominant; SE winds are low, not usable
4 Dec 2009	Narrow CZ at TG	Model overestimated	Wind weaker to SE; model wind overestimated in the south
5–6 Dec 2009	Narrow CZ at TG	Model predicted well	Wind weaker to SE, not usable
7 Dec 2009	Narrow CZ at TG	Model slightly overestimated	Wind overestimated to SE; weaker underestimated to NW; model wind slightly overestimated, not usable
20 Dec 2009	Narrow CZ at TG	Model underestimated	No information about winds
23 Dec 2009	Large CZ at TG	Model predicted well	Wind to NW is low; no information about SE wind, not usable
5 Jan 2010	Large CZ at buoy location	Model predicted well	Wind to NW is very low
19 Jan 2010	Narrow CZ at TG	Model overestimated	SE wind underestimated
20 Jan 2010	Narrow CZ at TG	Model predicted well	Both SE and NW winds are underestimated
3 Feb 2010	Large CZ at TG	Model overestimated	Winds are stronger in south; both SE and NW winds are underestimated
17 Mar 2010	Large CZ at TG	Model predicted well	Both SE and NE winds are strong; NW wind underestimated
18 Mar 2010	Large CZ at TG	Model overestimated	SE winds are stronger than NW; model well predicted

results, where the red-circled dot corresponds to the CZ shown in Figure 2. Given the information available, the estimated values in Figure 8 are only approximations of the truth. Nevertheless, from within these limits, under CZ conditions, the results strongly suggest a frequent underestimation of the model surface wind and an overestimation of significant wave height. Although limited by available data, similar trends are apparent for all the cases (two events were excluded due to a lack of wind data). More specifically, this supports our claim that when there is a CZ (i.e., when two wave systems move against each other—see the model and buoy two-dimensional spectra in Figure 9) model, wave heights are too large. This is the starting point for our discussion in the following section.

6. Analysis of Wave Model Source Functions Over CZs

Using results from the previous section, we analyzed the wind input (henceforth input) and dissipation by white-capping (w-c). Although our arguments do not have a theoretical foundation, they are based on physical intuition, sound reasoning, and previous results in the literature.

As pointed out in section 1, the wave modeling community tends to forget that the source functions for input and w-c were implicitly conceived, and later accepted, for an ideal wind-wave generation case. Although modifications/corrections have been suggested, mostly to consider the constant presence of swells in oceans, the overall framework remains the same. The w-c is of particular concern because its empirical expression remains the least known term of the energy balance equation and it sits at the base of any spectral wave model.

The classic, well-established method of testing the robustness of an approach is to test it in extreme or unusual situations, although still within the realm of possibilities, outside the ideal conditions it was founded on. The CZ in the Red Sea is an excellent opportunity for such a test (i.e., two well-developed wave systems, both wind generated, in approximately the same range of frequencies and energy, moving toward

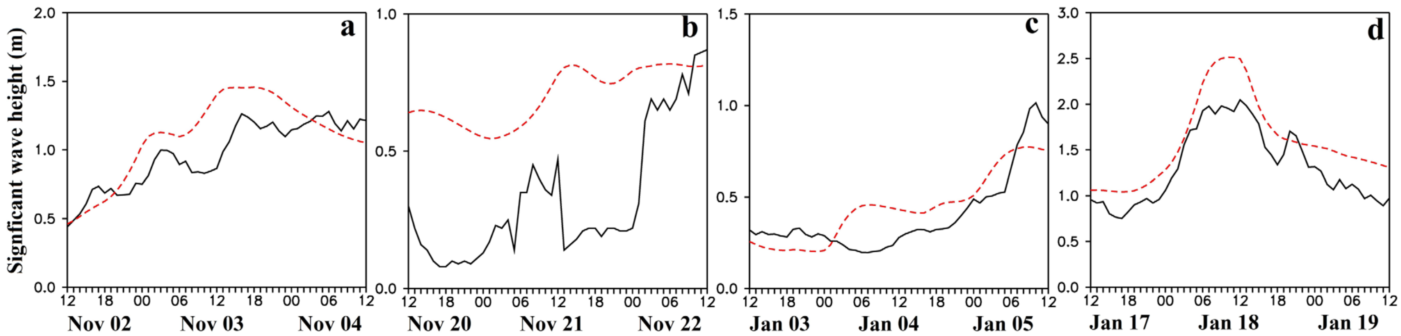

Figure 7. Three different cases of convergence recorded at the buoy location.

each other, and superimposed over a large part of the basin). Generally, a no-wind area divides the two windy zones (see the case in Figure 2), wherein some cases, for example in Figure 10, the two windy, and hence wave, zones meet. This typically occurs when the NW-blowing wind and wave fields cover the entire Red Sea, only to then be progressively pushed toward the south by colder, possibly more energetic, air entering from the Mediterranean Sea via the Gulf of Suez. In this case, the northerly SE-blowing cold air acts as a cold-front wedge, causing a full reversal of the direction of NW-blowing warmer air at the dividing surface line. This reversal causes the NW-blowing warmer system to slide on top of the colder SE-blowing system (see Figure 3). Because waves are an integrated effect in space and time, they exhibit smoother transition. The key point is that when on one side of the "front" system is wind driven, it produces a steep swell with a wide spectrum on the other side, and vice versa. Here we would like to point out that under these conditions, the physics of the situation are different from those commonly found in wave modeling. Consequently, some of the assumptions implicit in the accepted theories may not be fully valid. We aim to specify and, when possible, quantify the consequences.

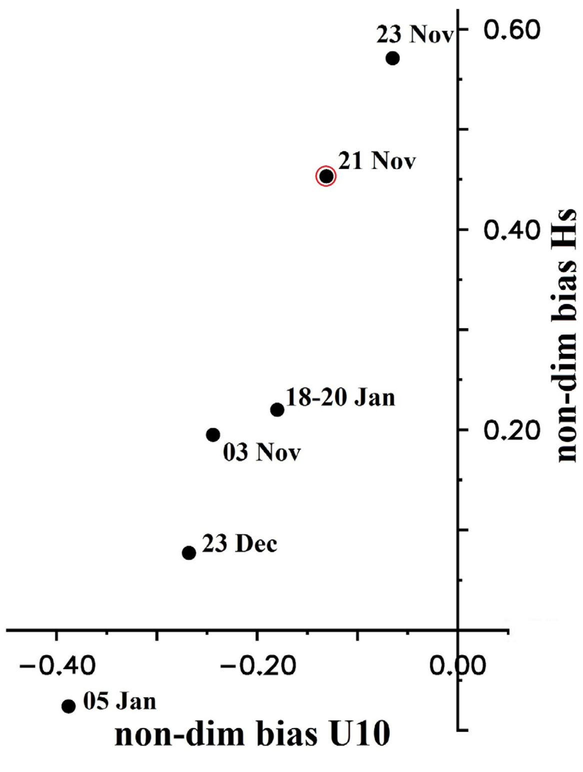

Figure 8. A scatterplot between adimensional percent H_s model errors versus buoy, and adimensional percent errors of enhanced (+7%) ECMWF 10 m wind speed versus scatterometer. The point with a red circle corresponds to the case in Figure 2.

We will start by examining at the input term of the model. The classical wave generation theories by the *Miles*' [1957] process, later improved by *Janssen* [1991], require an interaction between wind flow and the wavy field. Opposing wave conditions, as is the case in the Red Sea, causes a messy surface, similar to, but different from, the classical case of standing waves because of the presence of a full range of frequencies: crests are much sharper, continuously breaking in both directions, with an irregular motion that is quite different from the regular flow assumed in the model generation mechanism. The concept of a critical layer is not easily defined, and this is likely true over limited time and space in the CZ (i.e., until one of the two systems dominates). Nevertheless, it seems reasonable to assume that such a situation affects the generation process, decreasing its efficiency. The effect of an opposing swell on local wind sea generation has been studied in the Gulf of Tehuantepec (Mexico) [see, among others, *García-Nava et al.*, 2012]. It has been suggested that opposing swell decreases the input to the wind sea. Because

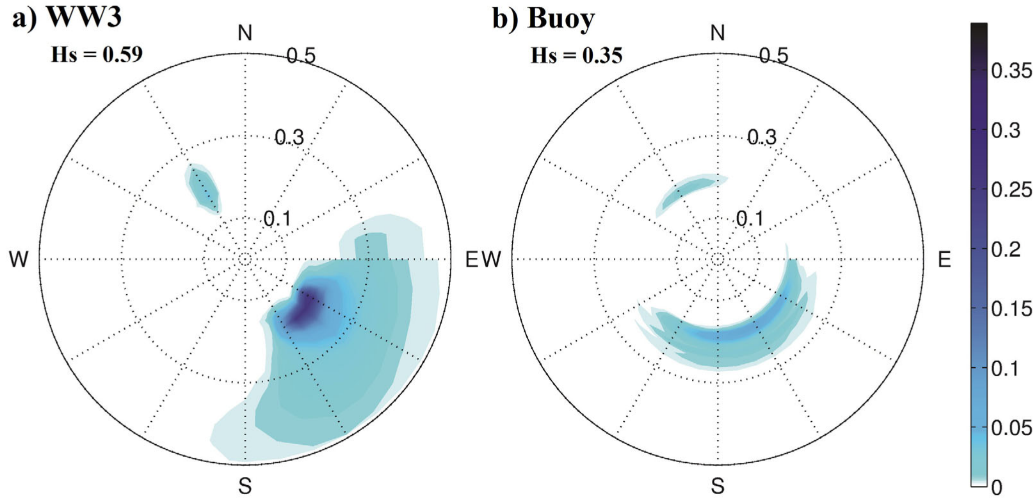

Figure 9. Observed and modeled 2-D spectra at 06 UTC 21 November 2009. Units are in m^2 s rad^{-1}.

of the stronger and more irregularly distributed deformation of the sea surface, this effect is likely to increase substantially (i.e., input is further reduced) when the two systems are in the same range of frequencies and/or with comparable energies.

By analyzing one of our cases in detail, we can clarify the type of situation that could be encountered. For example, Figure 10 illustrates the wind flow convergence from 18 to 19 January 2010.The position of the front is marked at 6 h intervals starting from 18 00 UTC when the front entered the Red Sea from the North. Figure 11 provides a general view of the conditions at the same time of Figure 10, showing how the energy of the two systems varied along the axis of the basin. Note that, although we are formally dealing with variance, we take the liberty of using the word "energy" because we believe it better conveys the feeling of the situation.

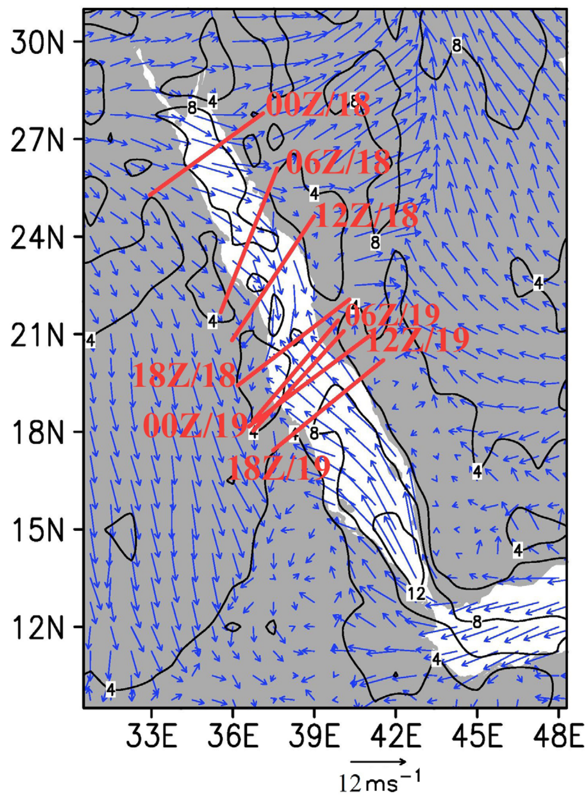

Figure 10. Typical wind flow convergence during the 18–21 January 2010 event. The red lines indicate the sequential, from north to south, frontal positions of the NW winds at labeled days and times. The plotted field is at 18 UTC 18 January 2010.

Figure 11c shows the progressive decay (seen by the model) of the NW system toward the north and the corresponding distribution of the SE system. Instead of growing with fetch, the SE system shows a uniform distribution in space until it reaches the position of "front." Then the SE system decays completely as it is moving against the vigorous north going flow. The more detailed view of the two systems presented in Figure 12 makes the progressive evolution in space of the two opposing systems evident. This is the situation for the front at the position in Figure 10. It is then enlightening to look in detail at the evolution of wave height and at the source functions at the buoy position from the model and measured values. Figure 13 provides more detailed information about the total energy and source functions, which shows for the period 18.00–20.12 (dd.hh):

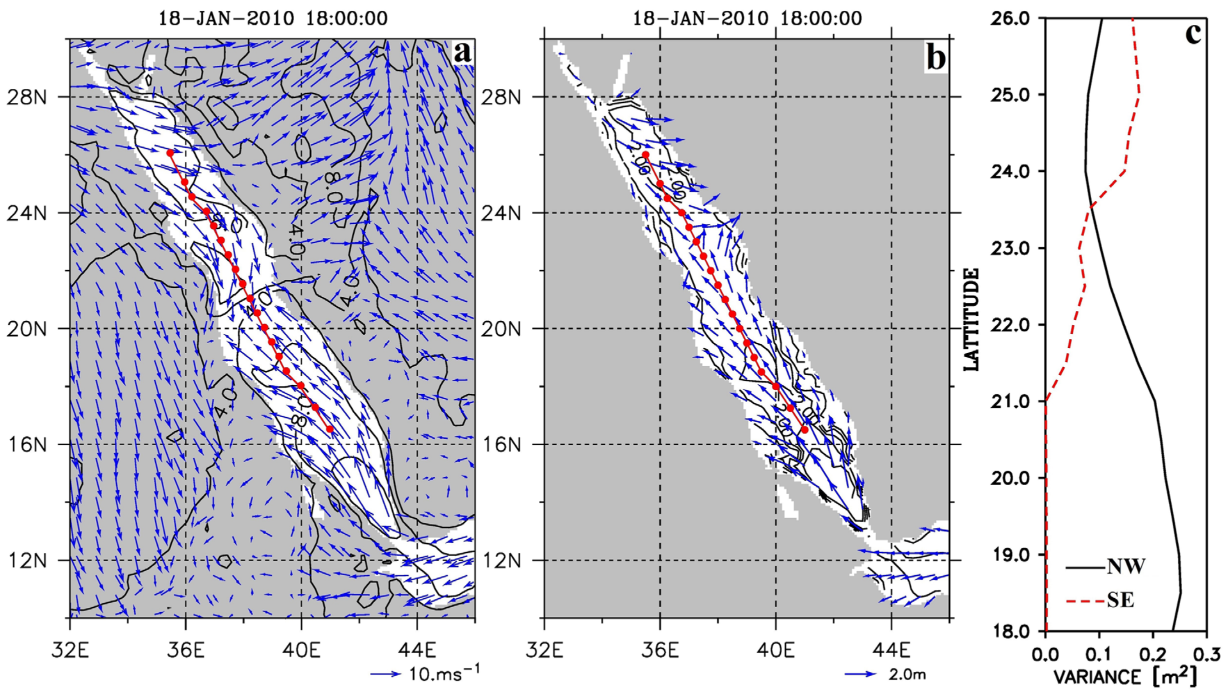

Figure 11. (a) Wind speed and (b) significant wave height fields during the convergence event of 18 January 2010. (c) Total energy (variance) of the two wave converging systems along the line shown in Figures 11a and 11b.

plot (a) the evolution of buoy and model overall energy, NW, and SE systems; (b) the total input, w-c energy, and their difference; (c) the same as (b) but for the NW system; and (d) the same as (b) but for the SE system. Using Figure 12 as a reference, the two systems have been quantified by splitting the two-dimensional

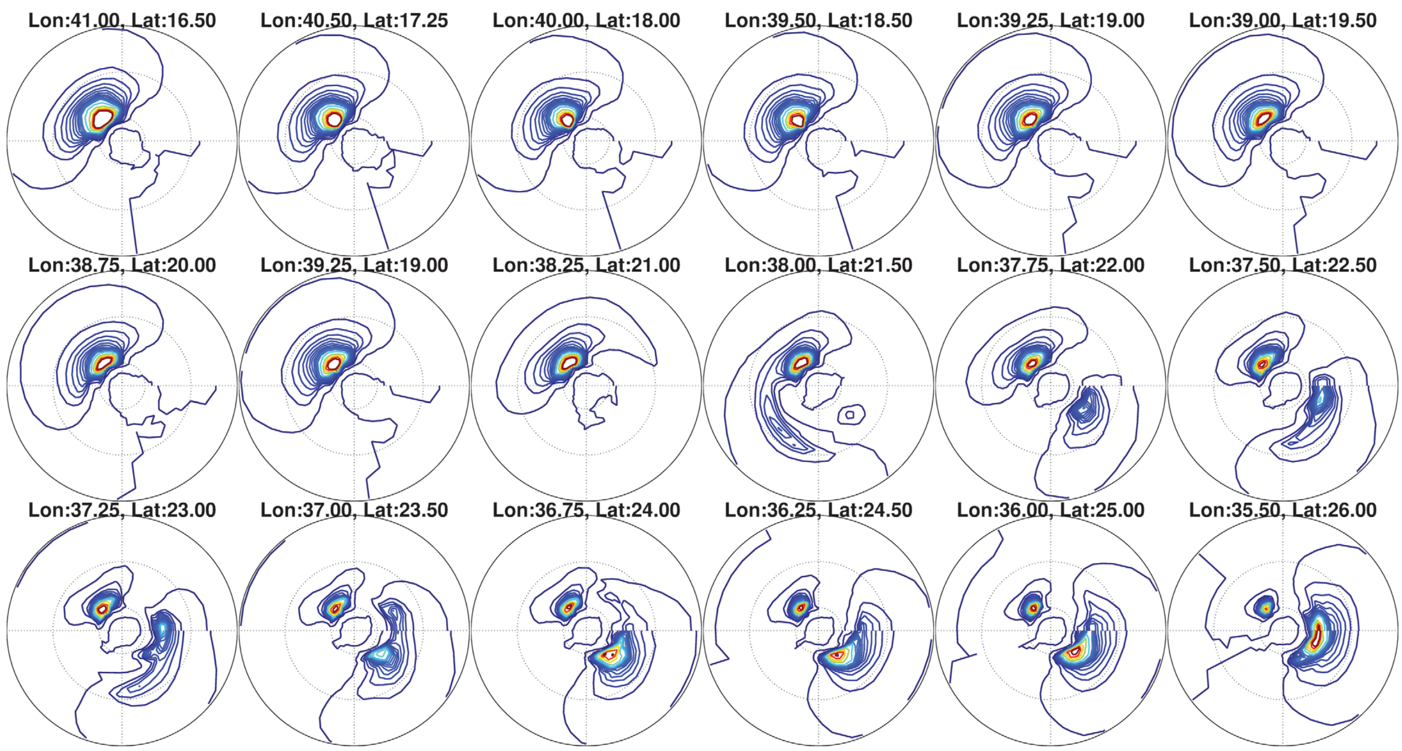

Figure 12. 2-D wave model spectra (m^2 s rad^{-1}) along the NW-SE line across the convergence zone at 18 UTC 18 January 2010. See Figure 11 for the distribution of points.

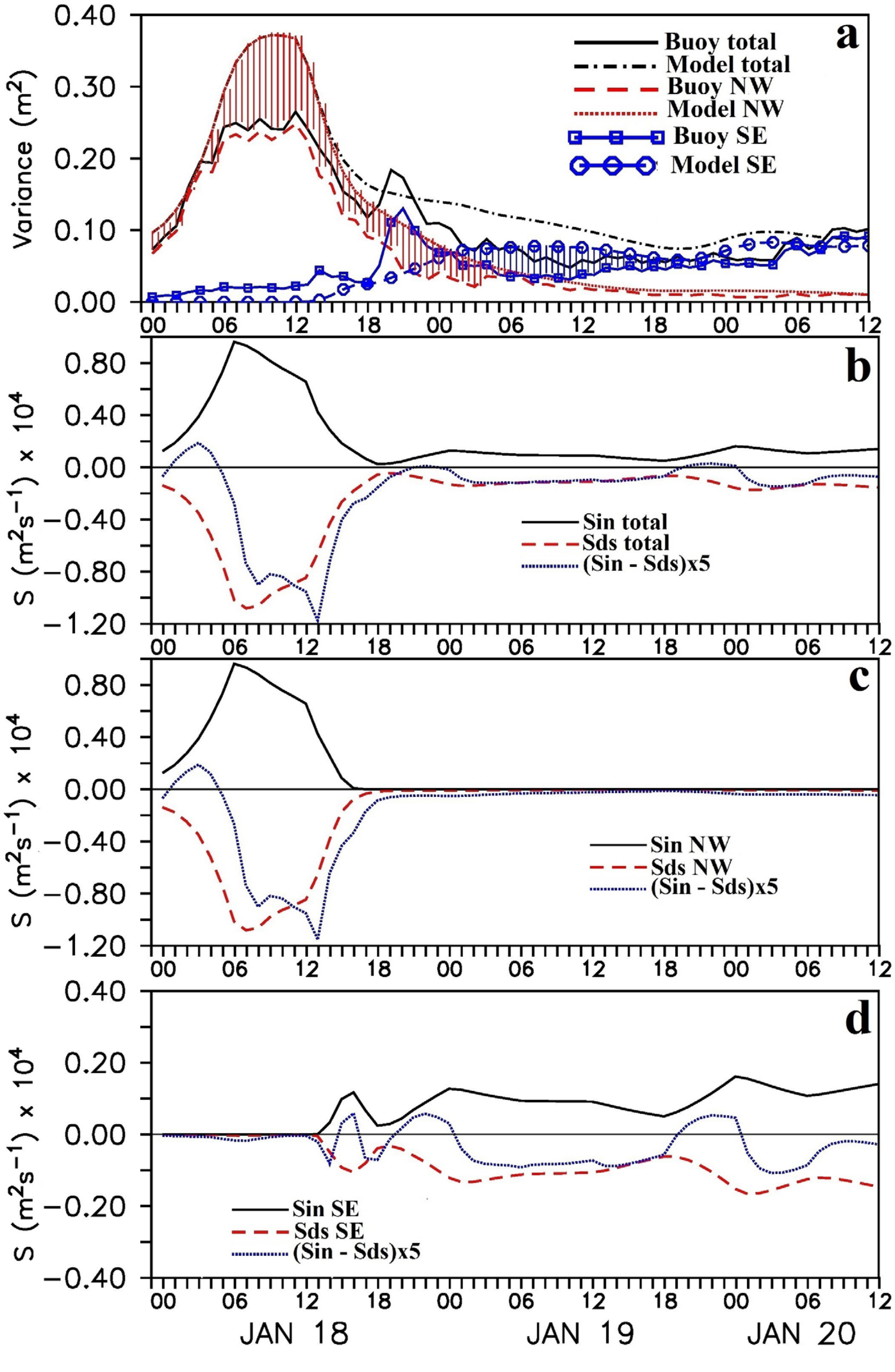

Figure 13. Total energy (variance) and source wind input and dissipation functions at the buoy location for NW and SE propagating wave systems. The shadowed areas show the excess energy of the modeled NW (red) and SE (blue) systems. See Figure 1 for the position of the buoy.

spectra along the 60°–240° line. Note that for a better visualization of plots (b)–(d), the differences have been multiplied by 5. A more detailed view is provided in Figures 14a and 14b, showing the frequency distribution of the source functions (input, w-c, nonlinear interactions (S_{nl}), and overall budget) at 18.00 and 19.12, respectively. The corresponding two-dimensional distributions (f-θ) are plotted in Figure 15.

Starting from Figure 13a, the large excess of the model NW system on the 18.00 (red shadowed area) is not supported by the source functions (Figures 13c and 14a), which suggests a strong local dissipation. Thus, the local growth at the buoy position is due to advection from the south that propagates unabated,

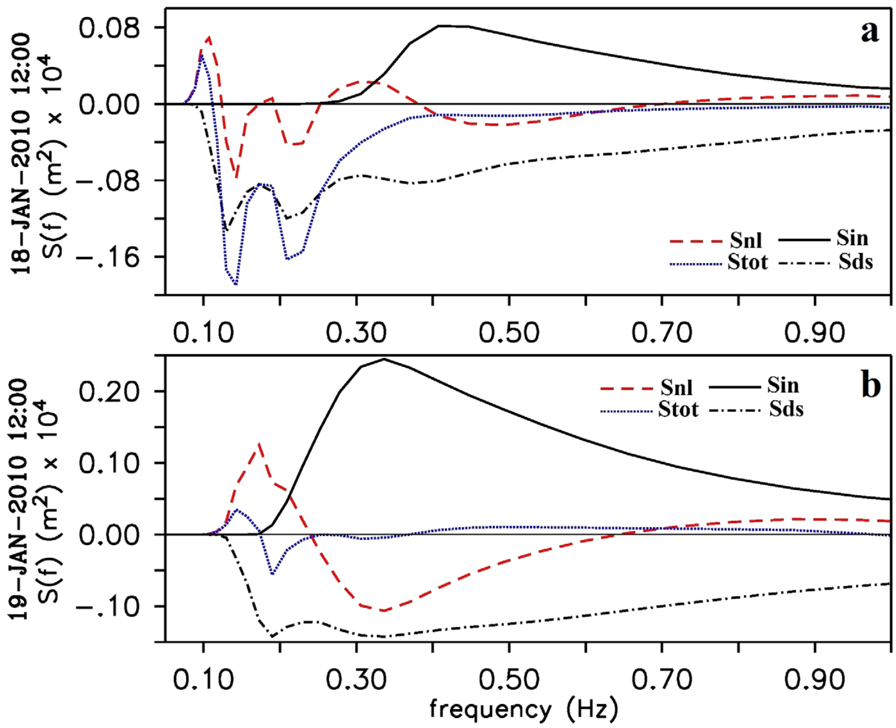

Figure 14. Source terms at the buoy location for 12 UTC 18 January and 12 UTC 19 January 2010.

although the waves are moving against a vigorous growing wind sea (Figure 15a). Note the two dissipation peaks (Figure 14a) and the two peaks of DIA (to be discussed latter).

The situation is opposite, but similar, at 19.12 (Figures 14b and 15b). As indicated in Figure 10, at this time the "front" line had moved south of the buoy, to the latitude of the Tokar Gap (see Figure 1). Figure 13a illustrates an energy excess from the growing SE system (the blue-shadowed area). However, the growth is not fully supported by the local source functions. A direct analysis places the previous front speed at about 30 km h^{-1} (i.e., close to 8 m s^{-1}, and the SE flowing waves at about 0.2 Hz peak frequency with a group speed of about 4 m s^{-1}). This indicates that the SE waves at the "front" were locally generated. After 19.00, when the front slowed down, the back SE waves catch up and increase the SE system behind the "front." Thus, the excess, with respect to the buoy, SE energy in Figure 13a on 19 January was again due to advection. Note that the available wind information from ASCAT indicates that the model winds were underestimated. The conclusion is that again the waves were advected unabated, without sufficient dissipation. Afterward the NW system decreases substantially, hence the interaction decreases and the model follows the buoy data without a particular bias.

7. The State of the Art and an Attempt for Correction

The unique wind and wave conditions in the Red Sea force the wave model to operate under conditions not considered when the different source functions were formulated. Here we used WW3, but it is clear that this is unessential because its physics is basically the same as in all the commonly available advanced wave spectral models. Because the problem is in the source functions, both input by wind and white-capping dissipation, the use of any third-generation wave model (e.g., WAM or SWAN) would have led to virtually the same results. Physical intuition, data analysis, and model results all suggest that in an unconventional situation (i.e., when two comparable wave systems move one against the other), the present formulations provide unsatisfactory solutions. Present and previous evidence suggests that in locations with environmental conditions such as those studied here, the present formulation, even in the state-of-the-art wave models, are biased toward an excessive input by wind and an underestimation of the loss by white-capping. *García-*

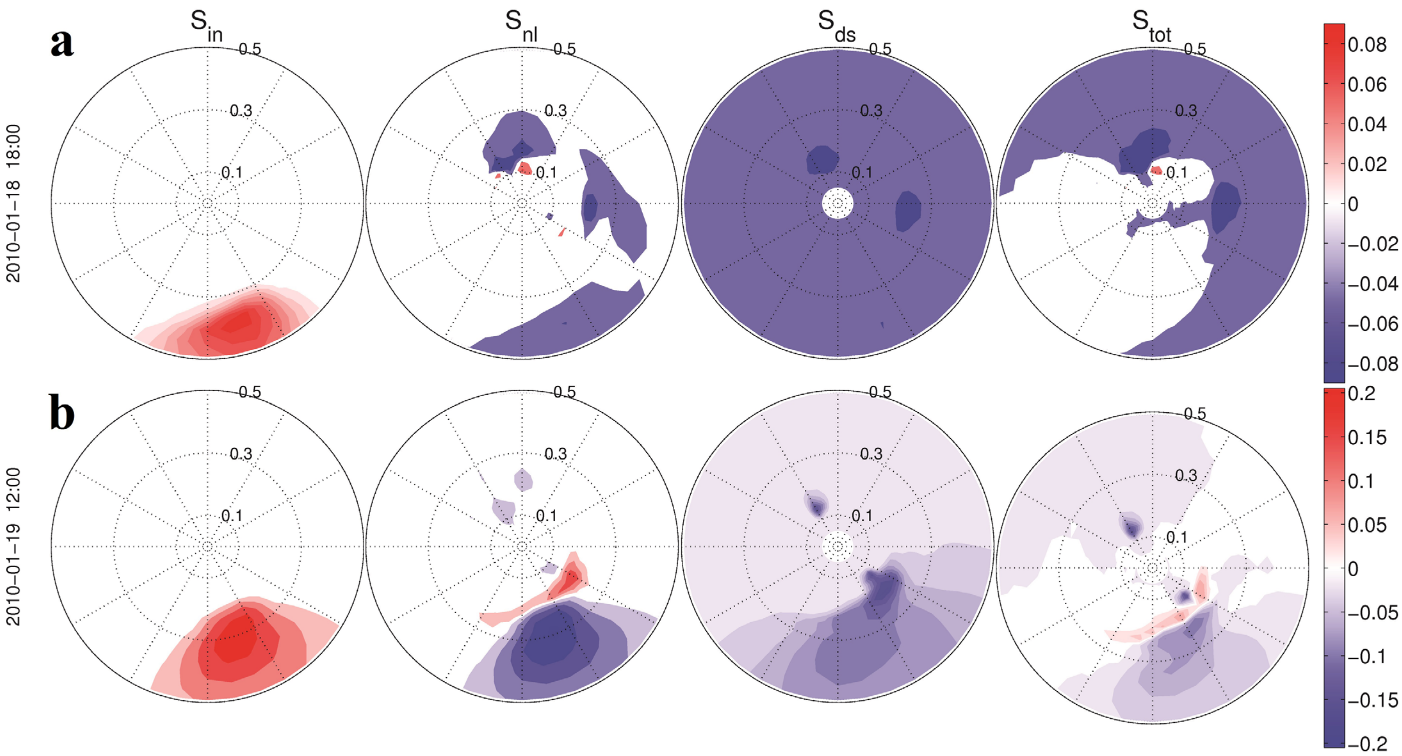

Figure 15. Source terms (m^2 rad^{-1}) at the buoy location for the convergence event of 18–19 January 2010. See Figure 1 for the position of the buoy.

Nava et al. [2012] have shown the influence of swell on an opposed growing wind sea, but we believe that the matter is substantially different when the two opposing systems are both steep and in the same range of frequencies. Not surprisingly, a precise quantification is difficult to define, and an analysis would require revisiting the background theory. Although the present approaches for white-capping contain more empiricism, there is room for improvements in this area as well.

Here we have outlined the problem, but we cannot separate the two effects because both are working in the same direction (i.e., toward decreasing wave heights). However, a recent work by *Cavaleri et al*. [2015] suggests that input by wind and white-capping should perhaps be seen as parts of a single process, and furthermore, to consider the influence of breaking waves on the generation by wind. This approach provides an opportunity to bypass the fundamental difficulty of modeling wave growth as a function of a small difference between wind input and white-capping.

Leaving these inspiring considerations for the future, we ought to look for a solution for the time being. The problem is not limited to a more accurate simulation of the wave conditions in the Red Sea. We have seen that the overall performance is satisfactory, and that the CZ zones, especially the ones with adjacent opposing systems, are limited in space and time. We are striving, at least from a quantitative point of view, for a more complete formulation capable of better tackling the interactions of different wave systems in the ocean, especially if similar in frequency and in range of interaction with the local wind. Our overall quantification, including the ones in Figure 8, is currently only an approximation of the truth. Although tempting, we have not tried to fit a curve to these results because six cases represent a very limited sample. However, the direction for future investigations is evident, i.e., decreasing the wind input and enhancing dissipation in encounter situations. As a preliminary, crude attempt, we have modified the related model source functions as follows. Define E_A and E_B as the energy of the two opposing systems. Taking full advantage of their clear separation in the Red Sea, we considered the S_{sin} and S_{dis} source functions for a spectral component in (e.g., system A)

$$S_{\mathrm{sin}A}=[\ldots\ldots\ldots]\left(1-\alpha\left(\frac{E_B}{E_A}\right)\left(\frac{L_{\mathrm{short}}}{L_{\mathrm{long}}}\right)\right) \tag{1}$$

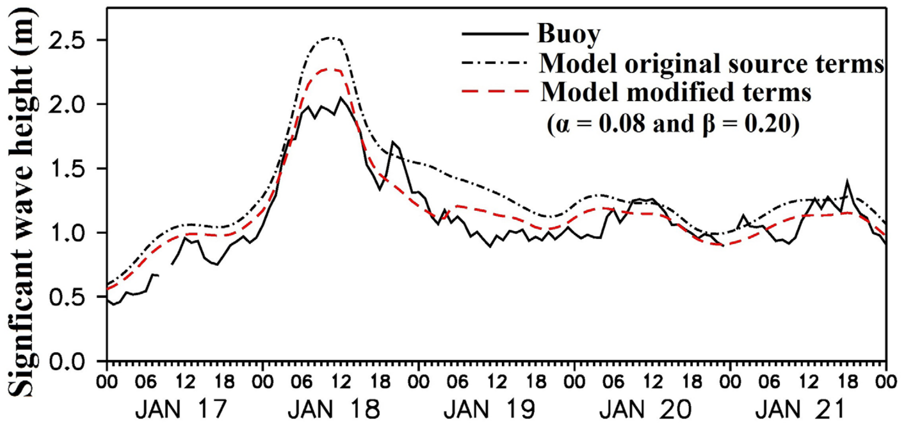

Figure 16. Significant wave height at the buoy location: from the buoy, modeled with original source terms, and with modified source terms with $\alpha = 0.08$ and $\beta = 0.20$.

$$S_{disA} = [\ldots\ldots\ldots]\left(1+\beta\left(\frac{E_B}{E_A}\right)\left(\frac{L_{short}}{L_{long}}\right)\right) \quad (2)$$

where [. . . . .] indicates the presently used source function and the term in brackets ( ) represents the correction. The rationale behind (1) and (2) is that a negative influence on S_{sinA} will correspond to a positive for S_{disA}. Also, the negative influence on S_{sinA} will grow with the increase in energy of the opposing system B. The influence will also depend on the dominant wavelengths of the two systems and will increase as both systems approach the same value. The term (L_{short}/L_{long}) is the same for the influence of B on A or vice versa, where L_{short} is the shorter of the two wavelengths. These are derived by linear theory after evaluating the mean frequency of each system. The coefficients α and β have been chosen in the range of 0.05–0.15 and 0.10–0.30, respectively. This reflects our perception that w-c will be more seriously affected (i.e., enhanced) by the "encounter." The entire period of October 2009 until March 2010 has been simulated for a number of combinations of the α and β coefficients in the chosen range. The typical result, selected in correspondence with Figure 13, is shown in Figure 16. While some excess of the H_s model values persists at the peak, a substantial decrease from the original formulation and a much better fit to the recorded data is evident. The best results were obtained with $\alpha = 0.08$ and $\beta = 0.20$, with no strong sensitivity to the specific α or β values. The overall statistics for the 5 months and the 19 convergence cases are given in Table 2, including the model comparison with both satellite and buoy data. The comparisons show a clear improvement in terms of better agreement between model and measured data using the modified source functions, for the longer-term statistics and in particular at the peak.

We have not discussed yet the role and implications of nonlinear interactions (NL). These do not directly change the overall energy budget. However, the related redistribution, depending on the spectral shape and hence on the presence of the two systems, could have indirect effects on the amount of wind input and white-capping dissipation. This potentially adds a new dimension to the problem. Since the sensitivity of NL is limited to the variations of the spectrum, the redistribution of energy will be very sensitive to the specific situation. In this paper, we have explored the case of two opposing wave systems from the point of view of the operational models, mostly based on the DIA. We have seen how a reasoned modification of the input and output terms leads to improved results. Now we look at how well the DIA, an accepted approximation for the classical generation case, deal with the two converging systems. Figure 17 (courtesy

Table 2. Best Fit Slopes of Used Surface Wind Speeds Versus Scatterometer Data, and Model Results Versus Altimeter and Buoy Measured Data

	Altimeters			Buoy		
Period (mm.dd)	Wind	Original	Modified	Wind	Original	Modified
10.01–03.31	1.00	1.02	0.99	0.97	1.01	0.98
19 cases	0.99	1.05	0.98	0.98	1.03	0.97

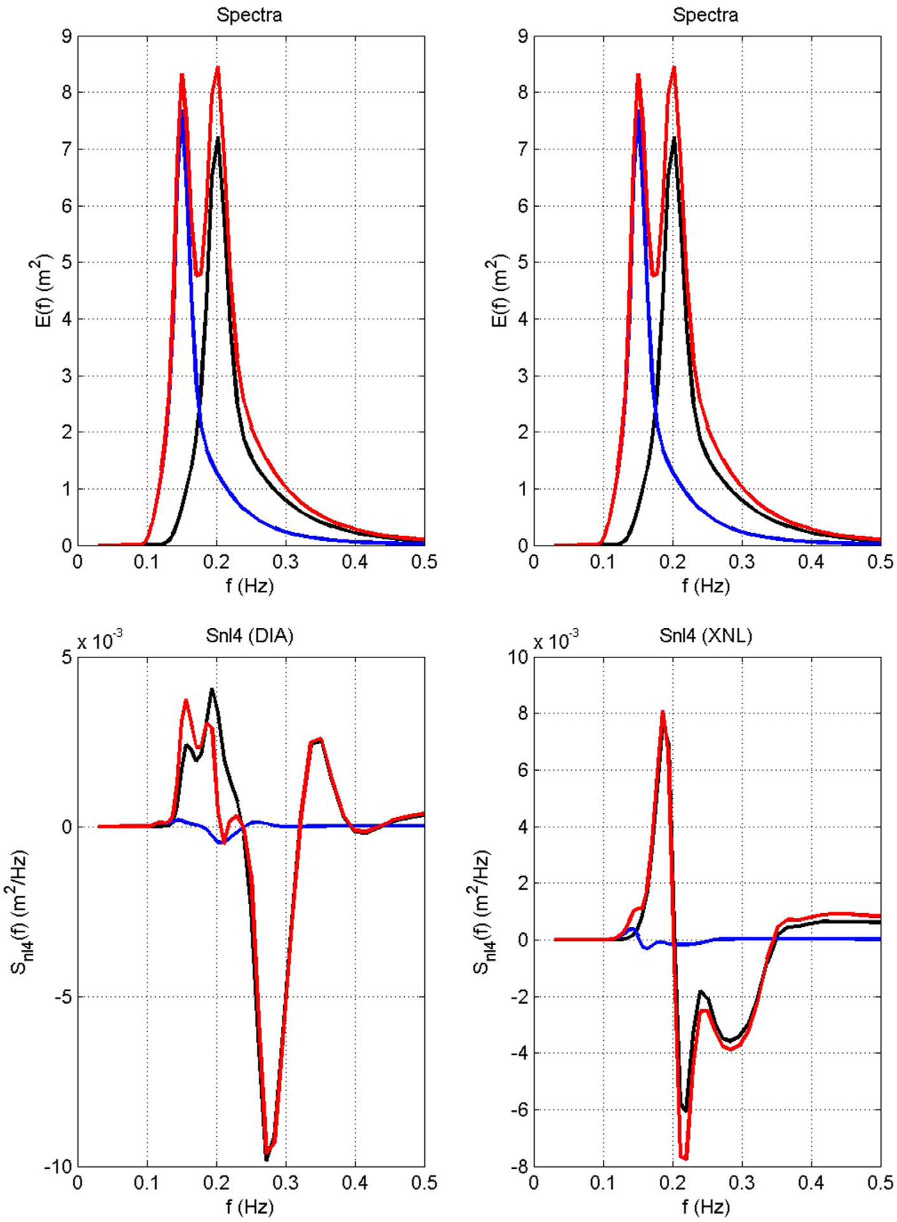

Figure 17. Two opposing wave spectra (top) with different peak frequencies 0.15 and 0.20 Hz and (bottom) their non-linear interactions with (left) DIA and (right) XNL. Black and blue curves show single spectra and their related (bottom) budget. Red curve shows the combined spectrum and the consequent (bottom) budget. The top plot is duplicated to allow a better interpretation of the NL differences with frequency. (Courtesy of Gerbrant van Vledder.)

of Gerbrant van Vledder) shows the nonlinear budget resulting from the use of DIA and the exact calculation (XNL). The black and blue lines show the two systems in the 1-D spectrum (top plots), the red one the overall system. The bottom plots provide, respectively, for DIA and XNL, the corresponding (single and combined) nonlinear budgets. Without entering the details (that would in any case change also for slight modifications of the situation), for the time being it suffices to note how different are the resulting DIA (left bottom plot) and XNL (right bottom plot) redistributions. Note in particular, how the XNL positive peak (at about 0.2 Hz) is to the right (higher frequencies) of the DIA one. Also the negative and high frequencies lobes are very different. The conclusion we derive is that, while the DIA, as repetitively proved, is a sufficient approximation for the more common situation of a dominant active wind sea, it does not cope well with more complicated situations, especially when, as in the present example, more than one active, more specifically steep, system is present.

8. A Discussion of the Results

In a recent paper, *Langodan et al*. [2014] reported positive results from the simulation of the wave conditions in the Red Sea, provided that the input ECMWF wind speeds were slightly increased. This is consistent with multiple previous results [see, among others, *Cavaleri and Bertotti*, 2004], indicating that, like other global model results, the ECMWF surface wind speeds are of good quality over the oceans, but have a marked tendency to underestimate the wind blowing from the coast, a fact relevant particularly in the inner seas.

A more focused examination of the wave model simulations in the Red Sea reveals that there is a tendency for wave models to overestimate the significant wave height within a period of the year repetitively characterized by the convergence of two opposing winds and related wave systems. It turns out that under these occasions, even with a correct or underestimated wind, the wave model tends to overestimate the wave conditions, particularly in the convergence zone. It is important to note that the two encountering wave systems, locally one under wind generation and the other out of a similar condition, have similar characteristics.

In our opinion, the overestimation is due to two parallel, but coacting, reasons with a common origin. On the one hand, the confrontation of the two systems profoundly modifies the surface conditions, making the generation by wind less effective. In parallel, the same situation leads to a substantially enhanced breaking with a consequently larger dissipation than anticipated by the generally accepted wave model formulation. However, this situation is not often present in the results reported by many users and specialists in operational centers; environmental conditions in the Red Sea are, if not unique, certainly very unusual. However, similar situations, at least with a similar potential problem, take place regularly also in the oceans. A classic example is a moving cold front, where the frontal wind, ahead of the front itself, is typically at angles of up to 90°, with respect to the motion of the front and the following wind. Modeling for these circumstances has long been a challenge to wave modeling and has been investigated since the SWAMP study [*The SWAMP Group*, 1985]. While at the time a great deal of attention was paid to the role of nonlinear interactions, in our opinion a similar problem as the one we have discussed exists. It is a matter of analyzing a model performance in specific areas, moments, and situations rather than at large scales.

From the physical point of view, maybe an improved definition of the physics of the source functions could be useful. The fact is that our evidence does not agree with the currently preferred approach, where, once the vertical wind profile has been established, the energy input to a spectral component depends only on the energy of that component. Instead, in certain conditions, the presence of other wave systems can also affect the input into that component. Similar, but different, arguments hold for white-capping.

Summarizing our findings and results:

1. The unusual, geometrical, and meteorological conditions in the Red Sea lead to wave conditions where the accuracy of the present formulation of the wave model source functions is in question.
2. Our wind and wave results suggest that the encounter of two wave systems in a meteorological convergence zone leads to less active wave generation by wind and more intense white-capping than predicted by the formulated model.
3. Less extreme, but similarly questionable situations are present in open oceans; for instance across a moving cold front. The finding, if we can tell it so, is that also in these less extreme situations the model formulation may not be adequate.
4. We have tentatively modified the input and white-capping source functions with a reduced generation and an enhanced dissipation depending on the characteristics, energy, and dominant wavelength of the two converging wave systems. The results support our assessment of the present wave modeling approach.
5. The DIA approach to nonlinear interactions is also shown to provide largely approximated results in these situations adding to the overall uncertainty.
6. Approaches along the line we have suggested may be a first and simple solution. However, in our opinion, the main result of this study is to show the limitations of the currently used formulations, and consequently the need for formulations capable of representing more complicated conditions of ocean waves, where the Red Sea convergence zone serves as only one example.

Acknowledgments

The research reported in this paper was supported by funding from King Abdullah University of Science and Technology (KAUST, Thuwal, Saudi Arabia). This research made use of the resources of the Supercomputing Laboratory and/or computer clusters at King Abdullah University of Science & Technology (KAUST) in Thuwal, Saudi Arabia. We thank J. Tom Farrar from Woods Hole Oceanographic Institution (WHOI, Woods Hole, Massachusetts, USA) and Yasser Abualnaja and Mohammedali Nellayaputhenpeedika from KAUST for assistance with the buoy data. Luigi Cavaleri took part to this study as part of the EU-funded MyWave project, Theme (SPA.2011.5-03). Figure 17 was kindly provided by Gerbrant van Vledder, Delft University of Technology). The data used in the study could be requested from the corresponding author (ibrahim.hoteit@kaust.edu.sa).

References

Ardhuin, F., E. Rogers, V. Babanin, J. F. Filipot, A. Roland, A. Van der Westhuysen, P. Queffeoulou, J. M. Lefevre, A. Lotfi, and F. Collard (2010), Semiempirical dissipation source functions for ocean waves. Part I: Definition, calibration and validation, *J. Phys. Oceanogr.*, *40*, 1917–1941.

Babanin, A. (2011), *Breaking and Dissipation of Ocean Surface Waves*, 463 pp., Cambridge Univ. Press, Cambridge, U. K.

Bidlot, J.-R., P. Janssen, and S. Abdalla (2007), A revised formulation of ocean wave dissipation and its model impact, *ECMWF Tech. Memo. 509*, 27 pp., Eur. Cent. for Medium-Range Weather Forecasts, Reading, U. K. [Available at http://www.ecmwf.int/publications.]

Cavaleri, L., and L. Bertotti (1997), In search of the correct wind and wave fields in a minor basin, *Mon. Weather Rev.*, *125*, 1964–1975.

Cavaleri, L., and L. Bertotti (2004), Accuracy of the modelled wind and wave fields in enclosed seas, *Tellus, Ser. A*, *56*, 167–175.

Cavaleri, L., L. Bertotti, and J.-R. Bidlot (2015), Waving in the rain, *J. Geophys. Res. Oceans*, *120*, 3248–3260, doi:10.1002/2014JCO10348.

García-Nava, H., F. J. Ocampo-Torres, P. A. Hwang, and P. Osuna (2012), Reduction of wind stress due to swell at high wind conditions, *J. Geophys. Res.*, *117*, C00J11, doi:10.1029/2011JC007833.

Hasselmann, K. (1974), On the spectral dissipation of ocean waves due to white capping, *Boundary Layer Meteorol.*, *6*, 107–127.

Hasselmann K., et al. (1973), Measurements of wind–wave growth and swell decay during the Joint North Sea Wave Project (JONSWAP), *Dtsch. Hydrogr. Z. A*, *8*(12), 1–95.

Hasselmann, S., K. Hasselmann, J. Allender, and T. Barnett (1985), Computation and parameterizations of the nonlinear energy transfer in a gravity-wave spectrum. Part II: Parameterizations of the nonlinear energy transfer for application in wave models, *J. Phys. Oceanogr.*, *15*, 1378–1391.

Janssen, P. A. E. M. (1991), Quasi-linear theory of wind wave generation applied to wave forecasting, *J. Phys. Oceanogr.*, *21*, 1631–1642.

Janssen, P. A. E. M. (2008), Progress in ocean wave forecasting, *J. Comput. Phys.*, *227*, 3572–3594.

Jiang, H., J. T. Farrar, R. C. Beardsley, R. Chen, and C. Chen (2009), Zonal surface wind jets across the Red Sea due to mountain gap forcing along both sides of the Red Sea, *Geophys. Res. Lett.*, *36*, L19605, doi:10.1029/2009GL040008.

Komen, G. J., S. Hasselmann, and K. Hasselmann (1984), On the existence of a fully developed wind-sea spectrum, *J. Phys. Oceanogr.*, *14*(8), 1271–1285.

Langodan, S., L. Cavaleri, Y. Viswanadhapalli, and I. Hoteit (2014), The Red Sea: A natural laboratory for wind and wave modeling, *J. Phys. Oceanogr.*, *44*, 3139–3159, doi:10.1175/JPO-D-13-0242.1.

Miles, J. W. (1957), On the generation of surface waves by shear flows, *J. Fluid Mech.*, *3*, 185–204.

Morcos, S. A. (1970), Physical and chemical oceanography of the Red Sea, *Oceanogr. Mar. Biol. Rev.*, *8*, 73–202.

Pedgley, D. E. (1966a), The Red Sea convergence zone. Part I—The horizontal pattern of winds, *Weather*, *21*, 350–358.

Pedgley, D. E. (1966b), The Red Sea convergence zone. Part II—Vertical structure, *Weather*, *21*, 394–406.

Teng, C. C., L. Bernard, B. Taft, and M. Burdette (2005), A compact wave and ocean data buoy system, in *Proceedings of MTS/IEEE OCEANS 2005*, vol. 2, pp. 1249–1254, IEEE, Washington, D. C., doi:10.1109/OCEANS.2005.1639926. [Available at http://ieeexplore.ieee.org/xpl/articleDetails.jsp?arnumber=1639926.]

The SWAMP Group (1985), *Ocean Wave Modeling*, 256 pp., Springer, U. S.

The WISE Group (2007), Wave modelling—The state of the art, *Prog. Oceanogr.*, *75*, 603–674, doi:10.1016/j.pocean.2007.05.005.

Tolman, H. L. (2008), User manual and system documentation of WAVEWATCH-III version 3.14, *Tech. Note 268*, pp. 25–32, NOAA/NWS/NCEP/OMB, Camp Springs, Md.